Check for updates

Bonding and stability of dinitrogen-bonded donor base-stabilized Si(0)/Ge(0) species [(cAAC^{Me}–Si/Ge)$_2$(N$_2$)]: EDA-NOCV analysis†

Harsha S. Karnamkkott, Sai Manoj N. V. T. Gorantla, [ID] Kavita Devi, Geetika Tiwari and Kartik Chandra Mondal [ID] *

Recently, dinitrogen (N$_2$) binding and its activation have been achieved by non-metal compounds like intermediate cAAC-borylene as (cAAC)$_2$(B-Dur)$_2$(N$_2$) [cAAC = cyclic alkyl(amino) carbene; Dur = aryl group, 2,3,5,6-tetramethylphenyl; B-Dur = borylene]. It has attracted a lot of scientific attention from different research areas because of its future prospects as a potent species towards the metal free reduction of N$_2$ into ammonia (NH$_3$) under mild conditions. Two (cAAC)(B-Dur) units, each of which possesses six valence electrons around the B-centre, are shown to accept σ-donations from the N$_2$ ligand (B ← N$_2$). Two B-Dur further provide π-backdonations (B → N$_2$) to a central N$_2$ ligand to strengthen the B–N$_2$–B bond, providing maximum stability to the compound (cAAC)$_2$(B-Dur)$_2$(N$_2$) since the summation of each pair wise interaction accounted for the total stabilization energy of the molecule. (cAAC)(B-Dur) unit is isolobal to cAAC–E (E = Si, Ge) fragment. Herein, we report on the stability and bonding of cAAC–E bonded N$_2$-complex (cAAC–E)$_2$(N$_2$) (**1–2**; Si, Ge) by NBO, QTAIM and EDA-NOCV analyses (EDA-NOCV = energy decomposition analysis coupled with natural orbital for chemical valence; QTAIM = quantum theory of atoms in molecule). Our calculation suggested that syntheses of elusive (cAAC–E)$_2$(N$_2$) (**1–2**; Si, Ge) species may be possible with cAAC ligands having bulky substitutions adjacent to the C$_{cAAC}$ atom by preventing the homo-dimerization of two (cAAC)(E) units which can lead to the formation of (cAAC–E)$_2$. The formation of E≡E bond is thermodynamically more favourable (E = Si, Ge) over binding energy of N$_2$ inbetween two cAAC–E units.

Introduction

The activation of small molecules[1] from natural resources has been an endless effort from scientists around the globe since the products could be utilised in certain ways for the survival of the human race[2] on earth and could even help to colonise the exo-planets in the future.[3] Small molecules like H$_2$, O$_2$, N$_2$, CO$_2$, CH$_4$, and others have initially been activated by different chemical species in the laboratory, and later on, some of the processes have been extended to the industrial scale.[4] Among the above-mentioned species, activations of N$_2$ and CH$_4$ have been considered to be the toughest due to their non-polar nature and kinetic inertness.[5] The N–N σ- and π-bonds of N$_2$, and C–H σ-bond of CH$_4$ are extremely stable and possess very high bond dissociation energies.[5] In addition, the electron pairs (bonding/anti-bonding electrons) which are available for σ-donation from these species (N$_2$ and CH$_4$) are quite low in energy and hence thermodynamically less favourable for the

formation of new bonds with the acceptors. Various research groups have isolated N$_2$-bonded complexes of early and late transition metals over the last two decades.[5c] The N–N triple bond in these complexes is stated to be activated and hence elongated due to the flow of electron densities from the metal's d-orbital to the π* of the N$_2$ ligand (Fig. 1).[5c] These metal complexes are engrossing since N≡N bond of a bonded N$_2$ complex is further elongated by stepwise additions of electrons and finally protons, leading to the formation of hydrazine (N$_2$H$_4$) or ammonia (NH$_3$).[5a,c] The former is utilised as a rocket fuel and the latter has a huge application in the fertiliser industry. Nitrogen containing fertilisers and bio-molecules are the most desired products for plants and micro-organisms or animals.[6] *Azotobacter*, which forms colonies in the roots of the plants, has the special and captivating ability to directly utilise aerial N$_2$ and reduce it to NH$_3$ catalysed by the inorganic cluster MoFe$_7$S$_9$C^{1-} (FeMoco) nitrogenase enzyme.[7,8] This process is linked to another cofactor, 4Fe–4S (P-cluster) residing within the same enzyme. The P-cluster provides the required number of electrons for the reduction of N$_2$ into NH$_3$. The overall process costs 16 Mg-ATP at ambient conditions.[7,8] This process has a huge impact on the survival of life on the planet, supplying billions of tonnes of nitrogen products by direct

Department of Chemistry, Indian Institute of Technology Madras, Chennai 600036, India. E-mail: csdkartik@iitm.ac.in

fixation of aerial N_2. A century ago, the Haber–Bosch process is the only industrial process by which 174 million tonnes of NH_3 are annually produced at present.[9] However, this process is energy-inefficient since it needs extreme conditions like high temperature and pressure (leading to the global warming *via* carbon emission). Several research groups have synthesised N_2-bonded main group elements complexes[10] and N_2-bonded metal complexes of different metal ions.[11–35] Most of them can catalytically reduce N_2 into NH_3 under mild conditions with low yield in the laboratory.

The compounds of main group elements have been unable to bind with N_2 for decades until recently an intermediate cAAC-borylene species of the general formula (cAAC)(B-Dur)[36] has been shown to bind with N_2 to produce $(cAAC)_2(B-Dur)_2(N_2)$ [cAAC = cyclic alkyl(amino)carbene;[37] Dur = aryl group, 2,3,5,6-tetramethylphenyl; B-Dur = borylene].[36] This remarkable species can be further treated with electron and proton sources to produce NH_3. However, this process is not cyclic possibly due to the stronger covalent bonding interaction between B- and N-atoms. There is a constant search for compounds of other or heavier main group elements that can mimic the N_2 reduction into NH_3 under milder conditions.

The E–N bond of heavier main group elements like Si and Ge are expected to be comparatively more dative in nature (E = Si, Ge) than the boron-analogue. In the past, carbene ligands (cAAC and/or NHC; NHC = N-hetero cyclic carbene) have been shown to form adducts [(L) → $ECl_{4−n}$; E Si, Ge; n = 0, 1, 2] with ECl_4/ECl_2. These adducts have been shown to be important synthons for the syntheses of Si_2 and Ge_2 units when the precursors have been reacted with suitable reducing agents. The cAAC has been established as a redox non-innocent and a stronger, π-accepting donor base ligand. It is not impossible to generate intermediate species cAAC → E (E = Si, Ge) which can possibly undergo dimerization and trimerization to produce cAAC → E = E ← cAAC and $(cAAC)_3E_3$ (E = Si).[38,39] The cAAC–E intermediate is isolobal with (cAAC)(B-Dur) (Fig. 2, left) and thus can be tested by

the EDA-NOCV method[40] to predict the stability of dinitrogen bonded dimeric species $(cAAC–E)_2(N_2)$ (**1–2**; E = Si, Ge; Fig. 2; right) (EDA-NOCV = energy decomposition analysis coupled with natural orbital for chemical valence). EDA-NOCV is a very powerful tool that can predict the quantum mechanical stability of chemical bonds[41] and hence can often predict the synthetic viability of a chemical species, although it cannot suggest a chemical route for the synthesis. There are several new classes of reactive species like carbone,[42] silylone and germylone whose stability has been predicted before their synthetic success. They were later synthesised and isolated in the laboratory; $(NHC)_2C(0)$.[43] Similarly, Frenking *et al.*[44a] predicted the stabilisation of a borylene-containing bulky ligand (B–R) *via* coordination with two CO ligands, and Braunschweig *et al.*[44b] have isolated it.

Computational methods

The optimizations of equilibrium geometries of **1** and **2** in singlet electronic states have been carried out at the BP86-D3(BJ)/Def2TZVPP level.[45] The absence of imaginary frequencies assures the minima on the potential energy surface. All the calculations have been performed using Gaussian 16 program package.[46] NBO[47] calculations have been performed using NBO 6.0 (ref. 48) program to evaluate partial charges, Wiberg bond indices (WBI) and natural bond orbitals (NBO). The nature of $Si–N_2$ and $Ge–N_2$ bonds of **1–2** have been analysed by energy decomposition analysis (EDA)[49] coupled with natural orbital for chemical valence (NOCV)[50] using ADF 2018.105 program package.[51] EDA-NOCV calculations were carried out at the BP86-D3(BJ)/TZ2P[52] level using the geometries optimized at BP86-D3(BJ)/TZ2PP level. EDA-NOCV method involves the decomposition of the intrinsic interaction energy (ΔE_{int}) between two fragments into four energy components as follows:

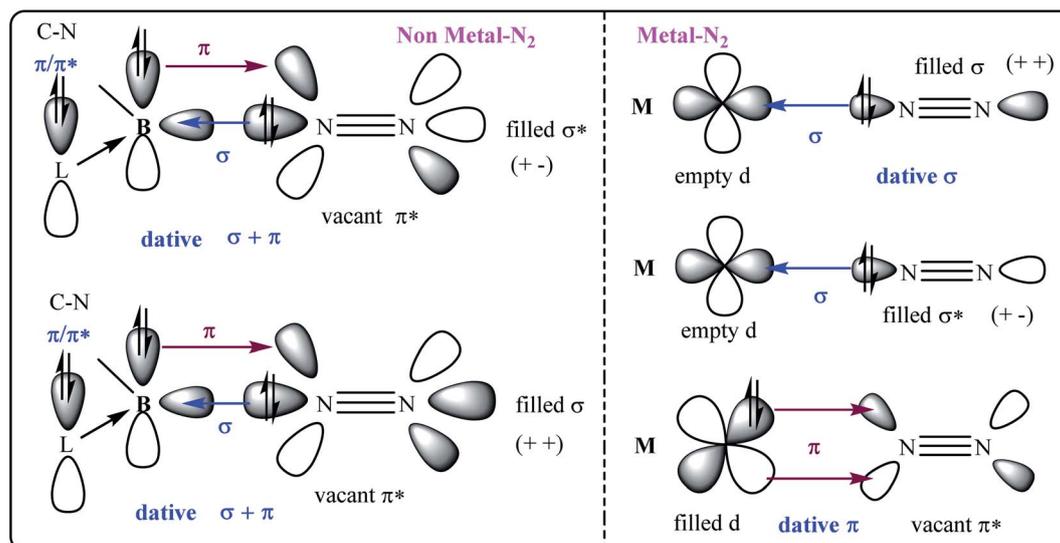$$\Delta E_{int} = \Delta E_{elstat} + \Delta E_{Pauli} + \Delta E_{orb} + \Delta E_{disp} \tag{1}$$

Fig. 1 The σ- and π-orbital interactions between orbitals of B and N_2 (left; non-metal–N_2); and, M and N_2 (right; metal–N_2). L = cAAC.
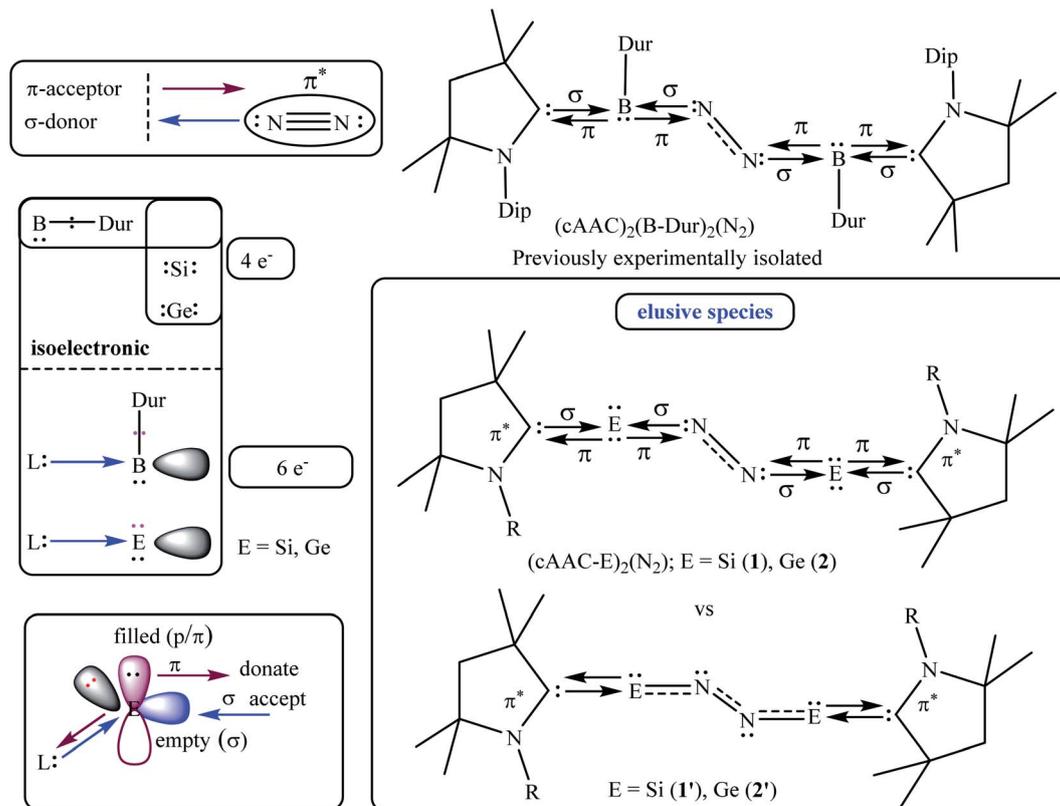
Paper

Fig. 2 The isoelectronic analogies of B–Dur, and (L)(B–Dur) with E, and (L)E [E = Si, Ge] (left), previously reported $(cAAC)_2(B-Dur)_2(N_2)$ (top, right), and elusive species $(cAAC-E)_2(N_2)$ (1–2; E = Si, Ge) (right, bottom).

where the electrostatic ΔE_{elstat} term is originated from the quasi-classical electrostatic interaction between the unperturbed charge distributions of the prepared fragments, the Pauli repulsion ΔE_{Pauli} is the energy change associated with the transformation from the superposition of the unperturbed electron densities of the isolated fragments to the wavefunction, which properly obeys the Pauli principle through explicit antisymmetrisation and renormalization of the production of the wavefunction. Dispersion interaction, ΔE_{disp} is also obtained as we used D3(BJ). The orbital term ΔE_{orb} comes from the mixing of orbitals, charge transfer and polarization between the isolated fragments. This can be further divided into contributions from each irreducible representation of the point group of the interacting system as follows

$$\Delta E_{orb} = \sum \Delta E_r \qquad (2)$$

The combined EDA-NOCV method is able to partition the total orbital interactions into pairwise contributions of the orbital interactions which is important in providing a complete picture of the bonding. The charge deformation $\Delta \rho_k(r)$, which comes from the mixing of the orbital pairs $\psi_k(r)$ and $\psi_{-k}(r)$ of the interacting fragments, gives the magnitude and the shape of the charge flow due to the orbital interactions (eqn (3)), and the associated orbital energy ΔE_{orb} presents the amount of orbital energy coming from such interaction (eqn (4)).
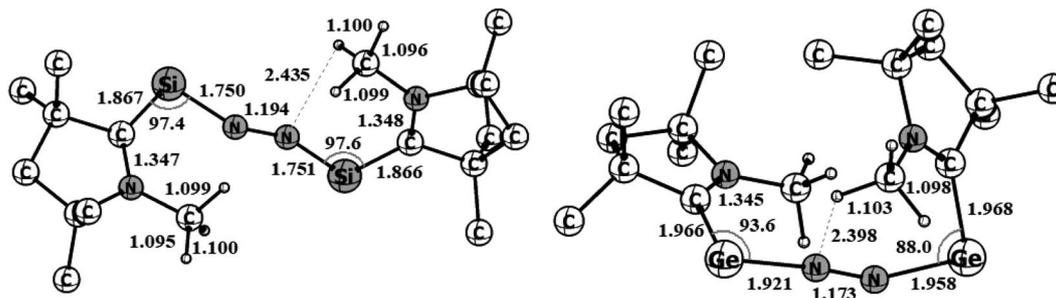

Fig. 3 Optimized equilibrium geometries of $(cAAC-Si)_2(N_2)$ (1) and $(cAAC-Ge)_2(N_2)$ (2) in singlet states at the BP86-D3(BJ)/TZ2P level of theory.

Table 1 Calculated bond lengths and angles at BP86-D3(BJ)/Def2TZVPP level of theory (Å)

Bond distance (Å)	$(cAAC–Si)_2(N_2)$ (**1**); E = Si	$(cAAC–Ge)_2(N_2)$ (**2**); E = Ge
C–N	1.347/1.348	1.345/1.349
C–E	1.867/1.866	1.966/1.968
E–N	1.750/1.751	1.921/1.958
N–N	1.194	1.173

Bond angles (°)	$(cAAC–Si)_2(N_2)$ (**1**); E = Si	$(cAAC–Ge)_2(N_2)$ (**2**); E = Ge
C–C–N	108.17	108.25
C–C–E	117.61	116.49
N–C–Si	134.22	135.11
C–E–N	97.42	93.61
E–N–N	154.18	163.58

$$\Delta\rho_{orb}(r) = \sum_k \Delta\rho k(r) = \sum_{k=1}^{N/2} \nu_k \left[-\psi_{-k}^2(r) + \psi_k^2(r) \right] \quad (3)$$

$$\Delta E_{orb} = \sum_k \Delta E_{orb}^k = \sum_k \nu_k - \left[-F_{-K,-K}^{TS} + F_{K,K}^{TS} \right] \quad (4)$$

Readers are further referred to the recent reviews articles to know more about the EDA-NOCV method and its application.[41]

Structure description

Geometry optimizations of $(cAAC–Si)_2(N_2)$ (**1**) and $(cAAC–Ge)_2(N_2)$ (**2**) at the BP86-D3(BJ)/Def2TZVPP level of theory revealed that both species have a singlet spin ground state (Fig. 3). The triplet states of both the species (**1–2**) are higher in energy by 12.2 (**2**) to 15 (**1**) kcal mol^{-1}. A notable observation is the disconnection of one Ge–N bond of $(cAAC–Ge)_2(N_2)$ (**2**) in its triplet state (Fig. S1†).

A μ-N_2 ligand has been coordinated by two cAAC^{Me}–E units in end-on fashion (E = Si, Ge). Si–N/Ge–N bond distances of **1**/**2** (1.75/1.96) are in between a covalent single bond and a double

bond. The lengths of the N–N bonds in **1–2** (1.194/1.173) are significantly longer than those of the free N_2 ligand (1.102). The C_{cAAC}–Si/Ge–N angles are in the range of 90° to 100° [97.4 (Si), 93.6(Ge)] which are significantly smaller than silylone/germylone (~117°; $(cAAC)_2E$; E = Si, Ge).[39b] The Si/Ge–N–N bond angles are 154.18° (Si) and 163.58° (Ge) suggesting that E–N_2–E unit is not perfectly linear. The E–N–N–E torsion angles are 109.68° (Si; **1**) and 140.19° (Ge; **2**). The C_{cAAC}–Si···Si–C_{cAAC} and C_{cAAC}–Ge···Ge–C_{cAAC} torsion angles are 107.81° (ref. 39a) and 67.19°, respectively, suggesting pseudo-*cis* orientations of cAAC^{Me} ligands with respect to the central E_2N_2 unit. The C_{cAAC}–N distances of the cAAC^{Me} ligands in **1–2** are nearly 1.35 Å suggesting the presence of π-backdonation[38,39] from E to C_{cAAC}-atom (Table 1).[39] The Me groups of two cAAC^{Me} ligands are *trans* to each other with respect to the central E–N_2–E unit (Fig. 3). The calculation of dissociation energy of E–N bond suggests that $((cAAC–E)_2N_2 \rightarrow 2 cAAC–E + N_2$; E = Si, Ge) Si–N bond (53.7 kcal mol^{-1}) in **1** is thermodynamically more stable than two Ge–N (35.7 kcal mol^{-1}) bonds in **2** by 18 kcal mol^{-1}. The Gibbs energy values of 28.3 kcal mol^{-1} (**1**) and 7.9 kcal mol^{-1} (**2**) indicates the endergonic nature of N_2 dissociation. A marginal increase in one of the C–H distances of N substituted methyl 1.100 (**1**) and 1.103 (**2**) is observed, indicating N–HC interaction.

The NBO calculations reveal that the Wiberg bond indexes (WBI) of Si/Ge–N bonds of **1–2** fall in the range of 0.71–0.91, while the same of N–N bonds of **1** and **2** are 1.82 and 2.04 respectively (Table 2). The reduced bond order of N–N bond is in accordance with the calculated bond lengths, suggesting the significant π-backdonation from the filled orbital of E (Si, Ge) to the vacant π*-orbital of the bridging N_2 unit. NBO analysis shows an electron occupancy of 1.97 e for the both Si–N bonds of **1**, which is polarised towards the nitrogen atom (84%). The results reveal an occupancy in the range of 1.98–1.99 e for the N–N bond in both species, with equal participation of both nitrogen atoms in the bond. The occupancy for the Ge–N bond of complex **2** was not provided by the NBO calculation, which could be due to low occupancy orbitals not exceeding the occupancy threshold value. The Ge–N bond might be a coordinate polar bond rather than a covalent coordinate donor–acceptor σ/π-bond (π Ge → N_{N2}; σ Ge ← N_{N2}). Further calculations show the concentration of charge on the N_2 unit in **1**

Table 2 NBO results of $(cAAC–E)_2(N_2)$ [E = Si (**1**) E = Ge (**2**)], (singlet state) at BP86/Def2TZVPP level of theory. Occupation number = ON, polarisation and hybridization of bonds and partial charge q. q_N = charges on each N-atom and q_{E_2} = charges on E_2 unit, q_{cAAC_2} = charges on cAAC$_2$ unit

Complex	Bond	ON	Polarisation and hybridisation (%)		WBI	q_N	q_{E_2}	q_{cAAC_2}
$(cAAC–Si)_2(N_2)$ **1**	Si′–N	1.97	Si′: 16 s(12), p(87), d(1)	N: 84 s(58.6), p(41.4)	0.91	−0.423	1.055	0.624
	Si′–N	1.97	Si′: 16 s(12), p(87), d(1)	N: 84 s(58.6), p(41.4)	0.91			
	N–N σ	1.99	N: 50 s(41), p(59)	N: 50 s(41), p(59)	1.82			
	N–N π	1.98	N: 49.6 s(1.2), p(98.8)	N: 50.4 s(1.3), p(98.7)				
	N–Nπ	1.98	N: 50.3 s(1), p(99)	N: 49.7 s(1), p(99)				
$(cAAC–Ge)_2(N_2)$ **2**	Ge′–N	—	—	—	0.76	−0.318	0.905	−0.539
	Ge′–N	—	—	—	0.71			
	N–N σ	1.99	N: 49.9 s(41), p(59)	N: 50.1 s(41), p(59)	2.04			
	N–N π	1.98	N: 49.2 s(0.2), p(99.8)	N: 50.1 s(0.2), p(99.8)				
	N–N π	1.98	N: 52.5 s(0.2), p(99.8)	N: 47.5 s(0.5), p(99.5)				
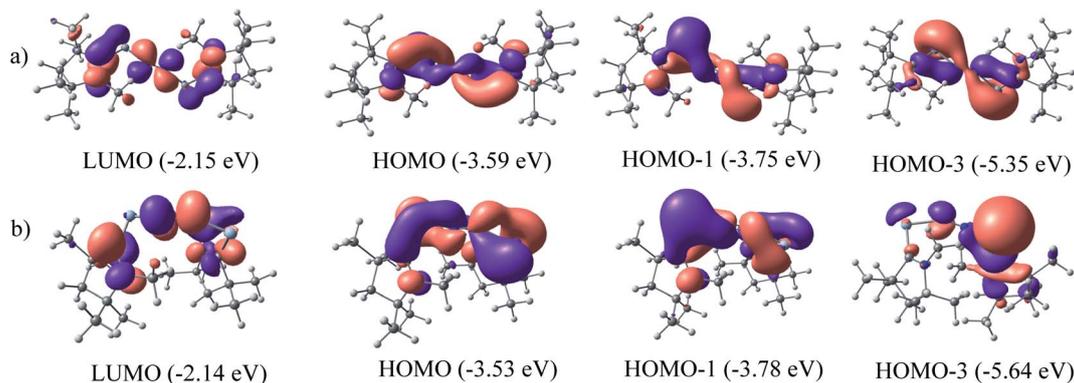
Fig. 4 NBOs of (a) (cAAC)$_2$Si$_2$N$_2$ (**1**) and (b) (cAAC)$_2$Ge$_2$N$_2$ (**2**) at BP86/Def2TZVPP level of theory.

(-0.846) and **2** (-0.636), signifying the flow of electrons from the E (Si, Ge) to N$_2$. Further, the positive partial charge on Si/Ge atoms agrees with the π-backdonation of electrons to the bonded N$_2$. However, cAAC ligands of compound **1** show overall positive charge, whereas the cAAC ligands of **2** show negative charge denoting a probable stronger cAAC ← Ge π-back-donation in **2**. The LUMO of **1** and **2** majorly represents the antibonding π*-orbitals on N$_2$ which are separated by nodes from two terminal E–C$_{cAAC}$–N$_{cAAC}$ units. HOMO and HOMO−1 suggest the lone pair of the Si/Ge atoms interact with the π*

orbital on the C$_{cAAC}$-atom as well as the central N$_2$ unit. HOMO−3 of **1** significantly denotes the interaction of a lone pair orbital with the N$_2$ π*-orbital, whereas in **2** HOMO−3 indicates the presence of a germanium lone pair orbital (Fig. 4). The HOMO–LUMO gap between these two species is in the range of 1.38–1.45 eV, indicating moderate electronic stability. In general, intra/inter molecular interaction may have effect on the conformations of these molecules. The intra molecular C$_{cAAC}$···C$_{cAAC}$ distances are 6.48 (**1**) and 5.08 (**2**) Å connecting themselves by a non-linear E–N$_2$–E chain. Any intramolecular
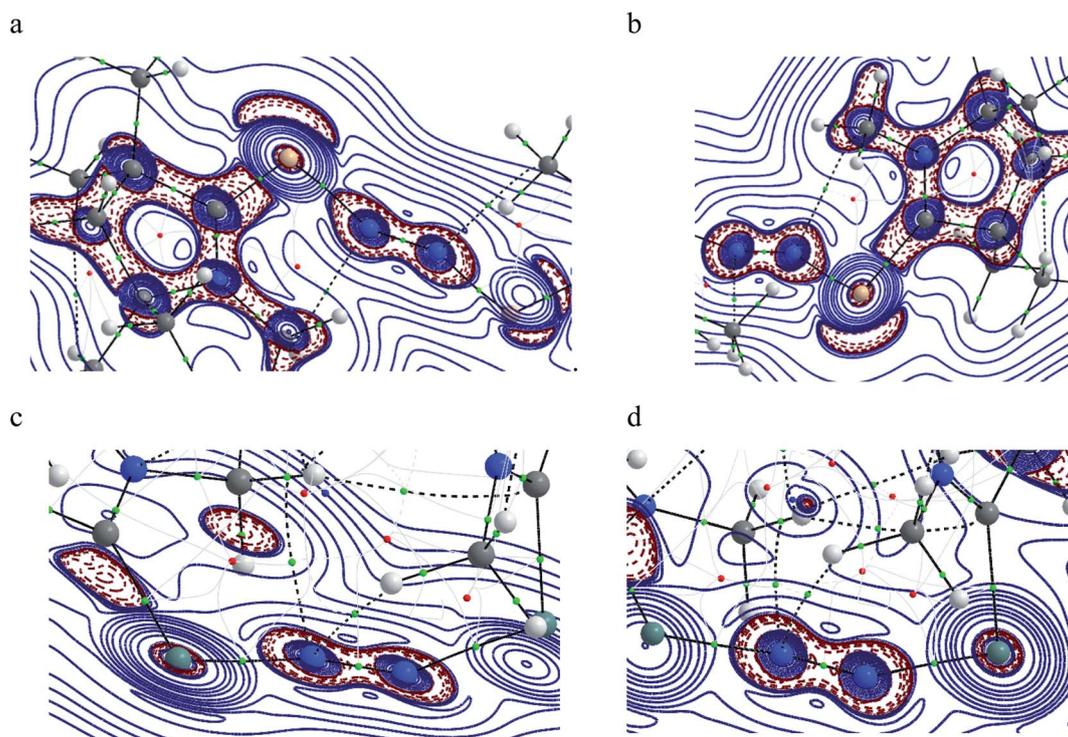

Fig. 5 Contour plot of Laplacian distribution [$\nabla^2\rho(r)$] in **1** and **2** in Si′−N−N and Si″−N−N (a and b) and Ge′−N−N and Ge″−N−N (c and d) bonds. Solid blue lines indicate the areas of charge concentration ($\nabla^2\rho(r) < 0$) while dotted red lines denote charge depletion ($\nabla^2\rho(r) > 0$). Solid lines connecting atomic nuclei (black) are the bond paths, small green spheres along the bond path are bond critical points (BCP), small red spheres denote the ring critical point and those thick solid blue lines separating the atomic basins indicates the zero-flux surface crossing the molecular plane. Blue coloured atoms represent N-atoms, white coloured atoms denoting hydrogen, brown coloured atom for Si, grey coloured atom for Ge respectively. Blue solid-line and dark solid-line represent charge accumulation and bond path while dotted line shows charge depletion.

Table 3 Electron density ($\rho(r)$), Laplacian ($\nabla^2\rho(r)$), total energy density ($H(r)$), potential energy density ($V(r)$), kinetic energy density ($G(r)$), ellipticity (ε_{BCP}), eta (η) values from QAIM analysis of $(cAAC)_2E_2N_2$ (E = Ge, Si) (singlet state) (the values are in a.u.)

Species	Bond	$\rho(r)$	$\nabla^2\rho(r)$	$H(r)$	$V(r)$	$G(r)$	ε_{BCP}	η
$(cAAC-Si)_2(N_2)$ **1**	Si′–N	0.107	0.538	−0.036	−0.207	0.171	0.155	0.190
	Si″–N	0.107	0.541	−0.036	−0.207	0.171	0.154	0.190
	N–N	0.524	−1.508	−1.031	−1.156	0.125	0.001	1.274
$(cAAC-Ge)_2(N_2)$ **2**	Ge′–N	0.099	0.391	−0.027	−0.152	0.125	0.140	0.199
	Ge″–N	0.093	0.327	−0.026	−0.133	0.107	0.127	0.206
	N–N	0.554	−1.652	−0.848	−1.284	0.435	0.005	1.33

Table 4 The EDA-NOCV results of dative (**D**) and electron sharing (**E**) at the BP86-D3(BJ)/TZ2P level of Si–N bonds of $(cAAC-Si)_2N_2$ (**1**) using neutral 2cAAC–Si fragment and neutral N_2 fragment in electronic singlet and quintet states as interacting fragments respectively. Energies are in kcal mol^{-1}

Molecule	Bond type	Fragments	ΔE_{int}	ΔE_{Pauli}	ΔE_{elec}	ΔE_{dis}	ΔE_{orb}
$(cAAC-Si)_2(N_2)$	**D**	**2cAAC–Si (S) + N$_2$ (S)**	**−68.1**	**395.6**	**−182.2**	**−6.6**	**−274.9**
	E	2cAAC–Si (Q) + N$_2$ (Q)	−424.1	354.5	−240.9	−6.6	−531.0

favourable interaction can bring some molecular units close to each other. NBO analyses show that the partial charges on N-atoms are −0.423 (**1**) and −0.318 (**2**). Significant CH$_{N-Me}$···N$_{N2}$ short contact (N$_{N2}$···H 2.49/2.51 (**1**), 2.39/2.55 (**2**); N$_{N2}$···C 2.81 (**1**), 2.80 (**2**) Å) is present. It might have brought two cAAC units of **1–2** relatively close to each other.

The QTAIM analysis of species **1–2** shows (Fig. 5 and Table 3) a higher positive value of Laplacian along the Si–N bond of complex **1** compared to the Ge–N bond of complex **2** denoting the depletion of electron density along the BCP, whereas the higher value of electron densities, $\rho(r)$ on the N–N bond of both complexes supports the charge migration calculated from NBO analysis. Besides, contour plots also reflect the higher concentration of electron densities on nitrogen atoms than on E (Si, Ge) atoms of both complexes. An imaginary bond path between the N$_2$ unit and the hydrogen of N-bound methyl group of cAAC in **1** and **2** is observed, indicating a possible N···HC$_{N-Me}$ interaction. The C–H$_{N-Me}$ bond lengths are in the range of 1.099 to 1.100 Å. The proximity to N-atom has been shown in optimized

geometries of **1–2** in Fig. 1. This N$_{N2}$ ($\delta-$)···($\delta+$) HC$_{N-Me}$ interaction could an electrostatic interaction since the partial charges on N-atoms of **1–2** significantly negative (Table 2).

The positive value of Laplacian at (3, −3) at topological point indicates a possible closed shell Si/Ge–N interaction. It is to be noted that the negative Laplacian for a covalent bond does not always hold true for bonds involving heavier elements like Si or Ge. However, the value of $|V(rc)|$ less than $2G(rc)$[53] and η value less than 1.0, further supports the Si/Ge–N closed shell interaction. The covalent nature of the N–N bond obtained from the negative value of its Laplacian and the total energy, denotes the bond stabilisation of the N$_2$ unit majorly through potential energy. Bond ellipticity is a measure of π character which is given by ($\varepsilon = (\lambda_1/\lambda_2) - 1$) at the topological point (3, −1).[54] For a single bond and triple bond, it reaches a value close to zero. The ellipticity value of the Si/Ge–N bond in both complexes indicates the possibility of the partial double bond character, whereas the value of N–N (0.001 and 0.005) indicates the

Table 5 The EDA-NOCV results at the BP86-D3(BJ)/TZ2P level of Si/Ge–N bonds of $(cAAC-Si)_2(N_2)$ (**1**) and $(cAAC-Ge)_2(N_2)$ (**2**) using neutral $(cAAC-Si/Ge)_2$ fragments and neutral N_2 fragment in electronic singlet states as interacting fragments. Energies are in kcal mol^{-1}. E = Si, Ge

Energy (kcal mol^{-1})	Interaction (σ E ← N$_2$, π E → N$_2$)	$(cAAC-Si)_2$ (S) + N$_2$ (S) 1	$(cAAC-Ge)_2$ (S) + N$_2$ (S) 2
ΔE_{int}		−68.1	−70.1
ΔE_{Pauli}		395.6	329.4
$\Delta E_{disp}{}^a$		−6.6 (1.4%)	−7.6 (1.9%)
$\Delta E_{elstat}{}^a$		−182.2 (39.3%)	−157.2 (39.4%)
$\Delta E_{orb}{}^a$		−274.9 (59.3%)	−234.6 (58.7%)
$\Delta E_{orb(1)}{}^b$	$(cAAC-E)_2 \to N_2$ π-backdonation	−74.1 (27.0%)	−119.7 (51.0%)
$\Delta E_{orb(2)}{}^b$	$(cAAC-E)_2 \to N_2$ π-backdonation	−66.5 (24.2%)	−41.9 (17.9%)
$\Delta E_{orb(3)}{}^b$	$(cAAC-E)_2 \gets N_2$ σ-donation	−56.6 (20.6%)	−25.4 (10.8%)
$\Delta E_{orb(4)}{}^b$	$(cAAC-E)_2 \gets N_2$ σ-donation	−42.8 (15.5%)	−20.1 (8.6%)
$\Delta E_{orb(5)}{}^b$	$(cAAC-E)_2$–N$_2$ σ-polarization	−9.4 (3.4%)	−8.3 (3.5%)
$\Delta E_{orb(rest)}{}^b$		−25.5 (9.3%)	−19.2 (8.2%)

^{a} The values in the parentheses show the contribution to the total attractive interaction $\Delta E_{elstat} + \Delta E_{orb} + \Delta E_{disp}$. ^{b} The values in parentheses show the contribution to the total orbital interaction ΔE_{orb}.
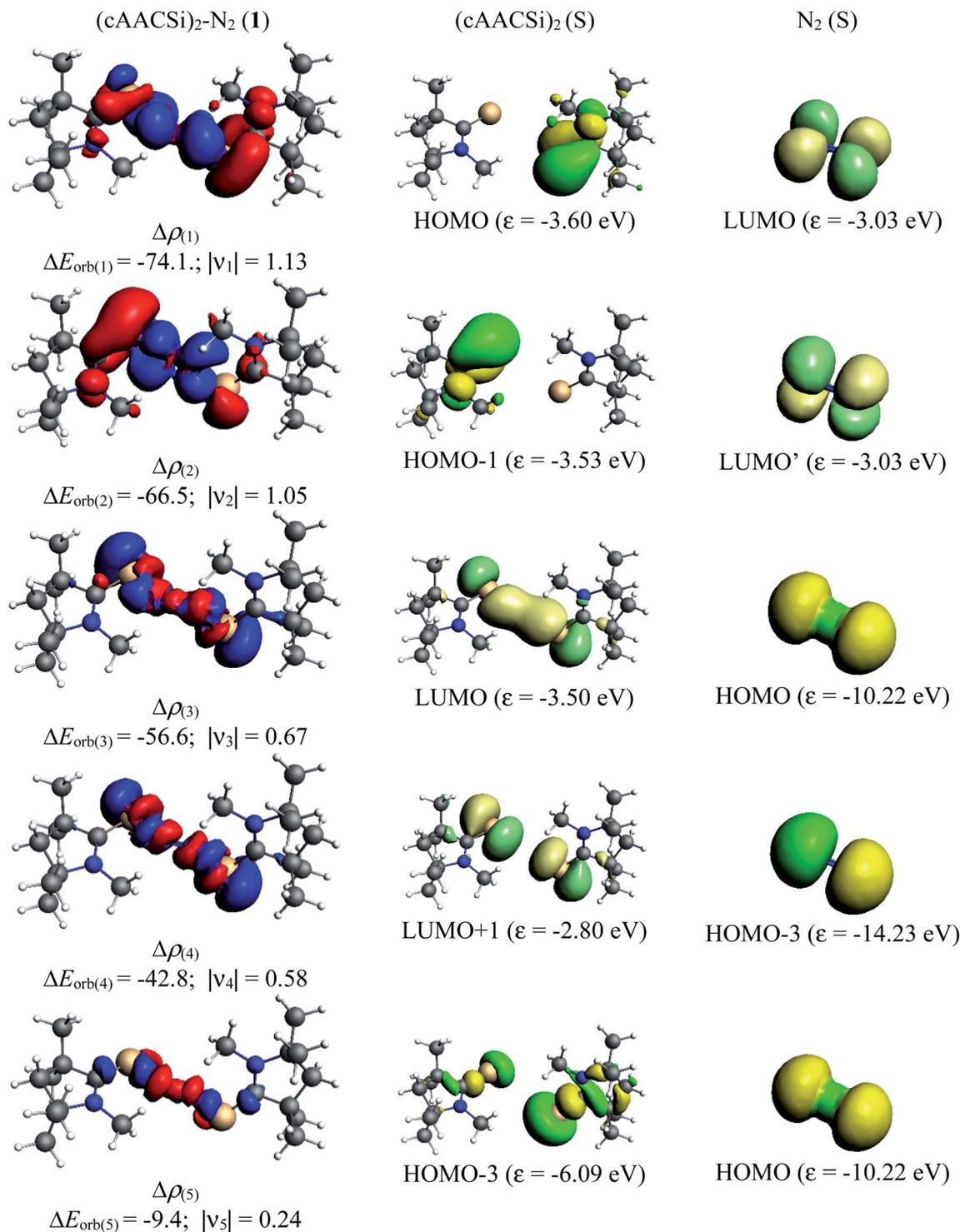
(cAACSi)$_2$-N$_2$ (1) (cAACSi)$_2$ (S) N$_2$ (S)

$\Delta\rho_{(1)}$
$\Delta E_{orb(1)} = -74.1.; |v_1| = 1.13$

HOMO ($\varepsilon = -3.60$ eV) LUMO ($\varepsilon = -3.03$ eV)

$\Delta\rho_{(2)}$
$\Delta E_{orb(2)} = -66.5; |v_2| = 1.05$

HOMO-1 ($\varepsilon = -3.53$ eV) LUMO' ($\varepsilon = -3.03$ eV)

$\Delta\rho_{(3)}$
$\Delta E_{orb(3)} = -56.6; |v_3| = 0.67$

LUMO ($\varepsilon = -3.50$ eV) HOMO ($\varepsilon = -10.22$ eV)

$\Delta\rho_{(4)}$
$\Delta E_{orb(4)} = -42.8; |v_4| = 0.58$

LUMO+1 ($\varepsilon = -2.80$ eV) HOMO-3 ($\varepsilon = -14.23$ eV)

$\Delta\rho_{(5)}$
$\Delta E_{orb(5)} = -9.4; |v_5| = 0.24$

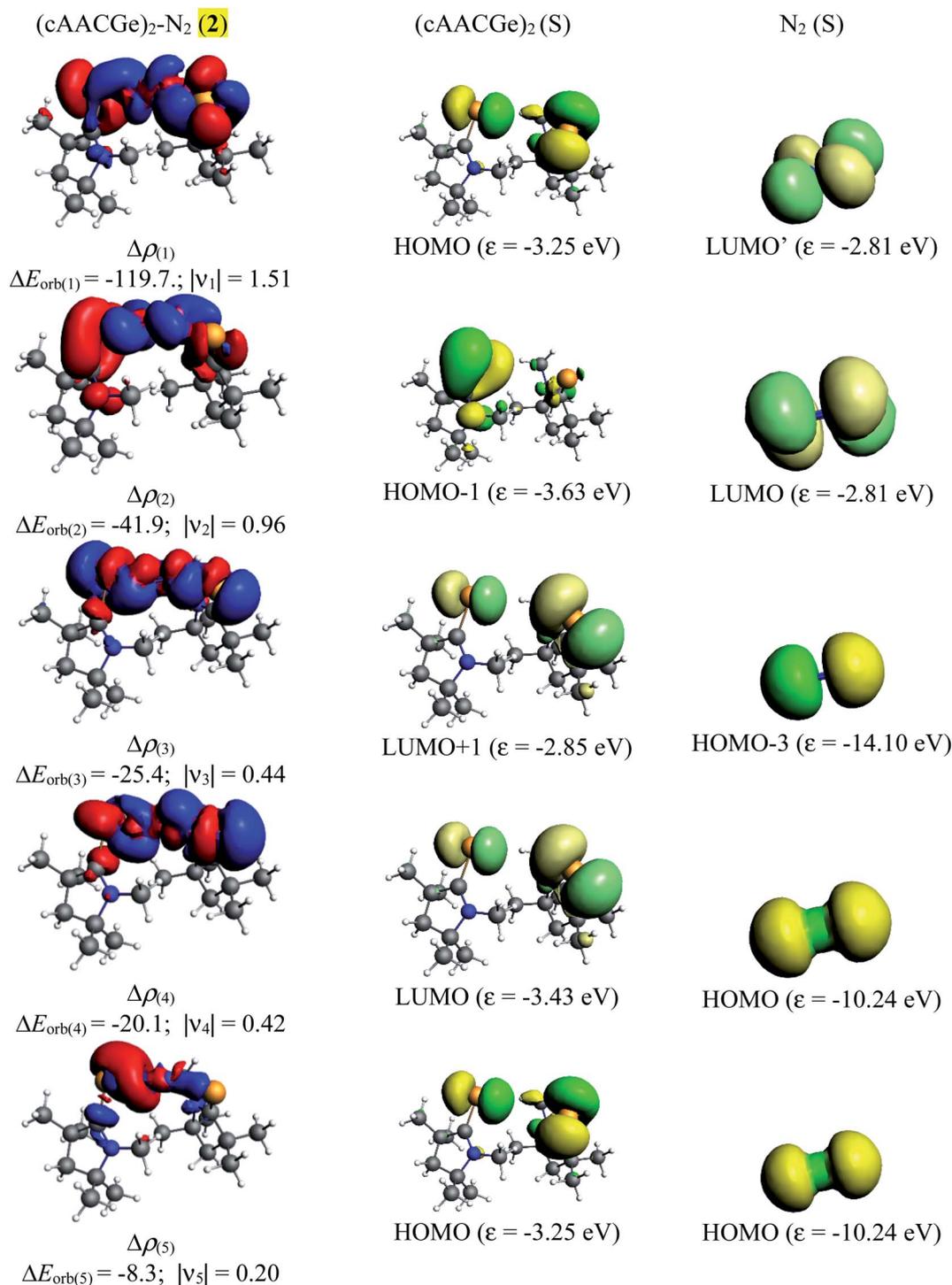HOMO-3 ($\varepsilon = -6.09$ eV) HOMO ($\varepsilon = -10.22$ eV)

Fig. 6 The shape of the deformation densities $\Delta\rho_{(1)-(5)}$ that correspond to $\Delta E_{orb(1)-(5)}$, and the associated MOs of (cAAC−Si)$_2$(N$_2$) (**1**) and the fragments orbitals of (cAAC−Si)$_2$ and N$_2$ in the singlet states at the BP86-D3(BJ)/TZ2P level. Isosurface values of 0.001 au for $\Delta\rho_{(1-5)}$. The eigenvalues v_n give the size of the charge migration in e. The direction of the charge flow of the deformation densities is red → blue.

cylindrically symmetric distribution of electron densities as expected for the N≡N bond.

NBO and QTAIM analyses however, cannot provide proper bonding scenarios and also cannot distinguish between an electron sharing covalent and a dative covalent bond. EDA-NOCV analyses of (cAAC)$_2$Si$_2$N$_2$ (**1**) and (cAAC)$_2$Ge$_2$N$_2$ (**2**) were carried out using methods similar to those reported for other species at the BP86/Def2TZVPP level of theory.[40–42,44a] The N$_2$-

$(cAACGe)_2-N_2$ **(2)**

$(cAACGe)_2$ (S)

N_2 (S)

$\Delta\rho_{(1)}$
$\Delta E_{orb(1)} = -119.7.; |\nu_1| = 1.51$

HOMO ($\varepsilon = -3.25$ eV)

LUMO' ($\varepsilon = -2.81$ eV)

$\Delta\rho_{(2)}$
$\Delta E_{orb(2)} = -41.9; |\nu_2| = 0.96$

HOMO-1 ($\varepsilon = -3.63$ eV)

LUMO ($\varepsilon = -2.81$ eV)

$\Delta\rho_{(3)}$
$\Delta E_{orb(3)} = -25.4; |\nu_3| = 0.44$

LUMO+1 ($\varepsilon = -2.85$ eV)

HOMO-3 ($\varepsilon = -14.10$ eV)

$\Delta\rho_{(4)}$
$\Delta E_{orb(4)} = -20.1; |\nu_4| = 0.42$

LUMO ($\varepsilon = -3.43$ eV)

HOMO ($\varepsilon = -10.24$ eV)

$\Delta\rho_{(5)}$
$\Delta E_{orb(5)} = -8.3; |\nu_5| = 0.20$

HOMO ($\varepsilon = -3.25$ eV)

HOMO ($\varepsilon = -10.24$ eV)

Fig. 7 The shape of the deformation densities $\Delta\rho_{(1)-(5)}$ that correspond to $\Delta E_{orb(1)-(5)}$, and the associated MOs of $(cAAC-Ge)_2(N_2)$ (**2**) and the fragments orbitals of $(cAAC-Ge)_2$ and N_2 in the singlet states at the BP86-D3(BJ)/TZ2P level. Isosurface values of 0.001 au for $\Delta\rho_{(1-5)}$. The eigenvalues ν_n give the size of the charge migration in e. The direction of the charge flow of the deformation densities is red → blue.

bonded silicon species $(cAAC)_2Si_2N_2$ (**1**) have been studied by two bonding scenarios (a) donor–acceptor dative (σ Si ← N_2, π Si → N_2; **1**) bond between $(cAAC^{Me}-Si)(Si-cAAC^{Me})$ and N_2 fragments in their singlet states, and (b) both σ- and π-electron sharing (Si=N–) bond (E) between $(cAAC^{Me}-Si)(Si-cAAC^{Me})$ and

N_2 fragments in their quintet states [like $cAAC^{Me}-Si=N-N=Si-cAAC^{Me}$; **1'**] (Fig. 2; middle). The minimum ΔE_{orb} is obtained (Table 4) for the former bonding scenario, confirming the preference of both dative (D) σ- and π-bonds between Si- and N-atoms of **1** over the electron sharing double bond as suggested
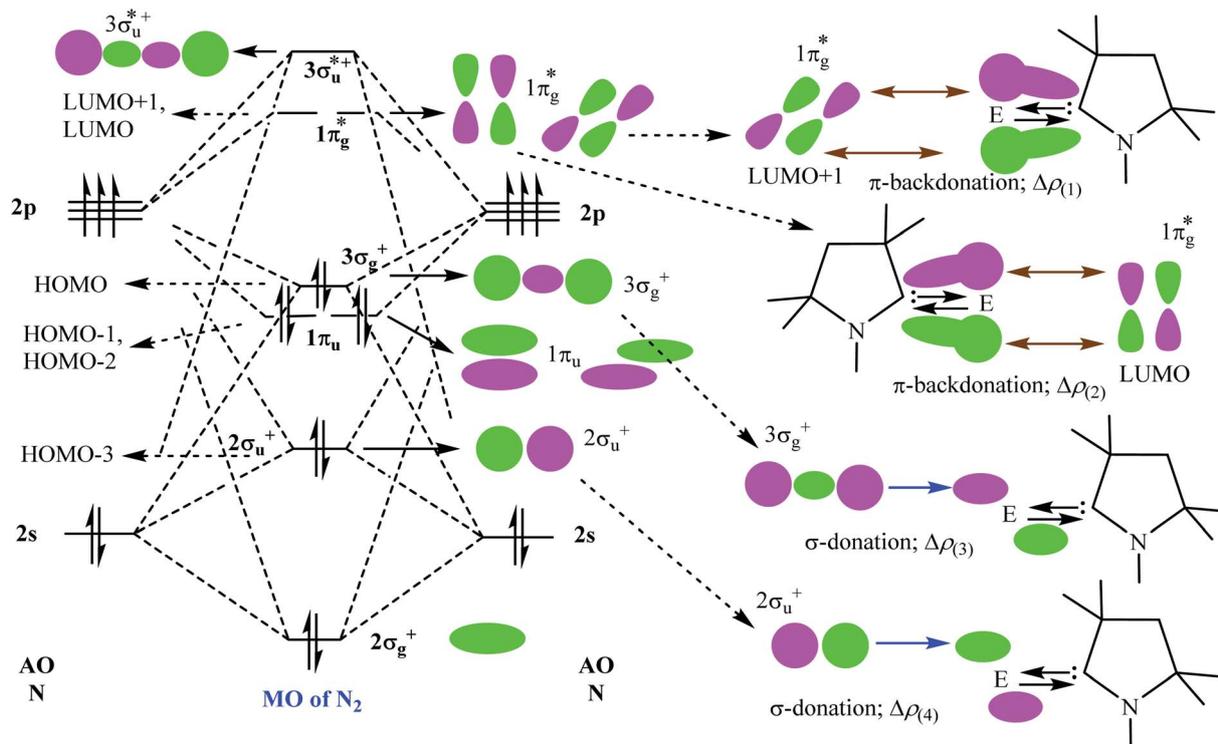
Fig. 8 Bonding and anti-bonding molecular orbitals of free N_2 molecule (left). The pairwise orbital interactions between few bonding and anti-bonding molecular orbitals of N_2 fragment with one of the cAAC^{Me}–Si fragments (right; for simplification one is shown).

for previously reported $(cAAC)_2(B\text{-Dur})_2(N_2)$ species.[36] A similar bonding scenario is expected for the comparatively more electron positive Ge-analogue (**2**). This correlates well with the charge distribution from the NBO analysis and closed shell bonding suggestion from the QTAIM results.

The bonding and stability of $(cAAC)_2E_2$ by EDA-NOCV analyses have been previously studied by Frenking *et al.*[55,56] The $(cAAC)_2$ fragment has been shown to form two strong dative σ-bonds with the E_2 unit [cAAC → E_2 ← cAAC]. In addition, there are two π-bonds (π-backdonation) between E_2 and $(cAAC)_2$ [cAAC ← E_2 → cAAC; E = Si, Ge]. The total intrinsic interaction energy is nearly −140 (E = Si)/−100 (E = Ge) kcal mol^{-1}.[55,56] The C_{cAAC}–N bond lengths in **1–2** are close to 1.35 Å which signifies moderate π-backdonation from E to cAAC [E_2 → cAAC].[38,39] The bonding interactions between (cAAC) and E have not been studied further here, as they have already been established (E = Si, Ge) before by Frenking *et al.*[55,56]

Table 5 shows that the intrinsic interaction energies of silicon and germanium species (**1–2**) are −68 to −70 kcal mol^{-1}, respectively. The Si-analogue (**1**) possesses significantly higher Pauli repulsion energy than Ge-containing species (**2**). Both the coulombic and orbital interactions in **1** contribute higher stabilization energies than those in **2**. Overall, ΔE_{int} indicates that Ge-species is slightly more stable (2 kcal mol^{-1}) than Si-species. The contribution due to orbital interaction (ΔE_{orb}) is significantly (∼59%) higher than coulombic (∼40%) interactions in both species **1–2**. EDA-NOCV provides an additional feature called pairwise orbital interaction which shows the

interacting orbitals of the fragments (Fig. 6 and 7). The total ΔE_{orb} is split into several major interacting sub-energies. The major orbital stabilization in **1** due to the formation E–N bonds comes from four significant orbital interactions [cAAC–E → N_2 ← E–cAAC, HOMO, HOMO−1 of $(cAAC–E)_2$ fragment to LUMO+1 and LUMO (doubly degenerate $1\pi_g$) of central N_2; Fig. 6–8]. These π-backdonations in **1–2** contribute 51% (**1**) and 69% (**2**), respectively, of total orbital interaction (ΔE_{orb}) (Fig. 6 and 7). The π-backdonations correlate well with the ellipticity values from QTAIM analysis. The MESP plots (Fig. 10) shows the charge accumulation (red region) in the E–N_2–E region while the charge shifted from cAAC ligands (bluish-green region). The σ-donations in **1–2** contribute ∼35% (**1**) and ∼20% (**2**), respectively, of total orbital interaction (ΔE_{orb}). The σ-charge polarizations in **1–2** contribute ∼9% (**1**) and ∼8% (**2**), respectively. In addition, 8–9% of the total interaction arises from other types of orbital interactions which are not negligible. The EDA-NOCV analyses suggest that cAAC–E unit can act as strong π-donor (π-orbital of N–C–E unit) towards the binding of molecule N_2 in **1–2**.

Finally, we tried to optimize the geometries of $(cAAC^{Me}–Si)_2(N_2)$ (**1**) and $(cAAC^{Me}–Ge)_2(N_2)$ (**2**) compounds with the ligands *trans* to each other. In case of compound **1**, two cAAC^{Me} ligands remained *trans* to each other through the optimization steps, though there were slight changes in the final low energy geometry. However, for compound **2**, the attempt to optimize *trans*-geometry interestingly resulted in a final *cis*-geometry. The plots of energy *vs.* optimization steps have been shown in Fig. S2
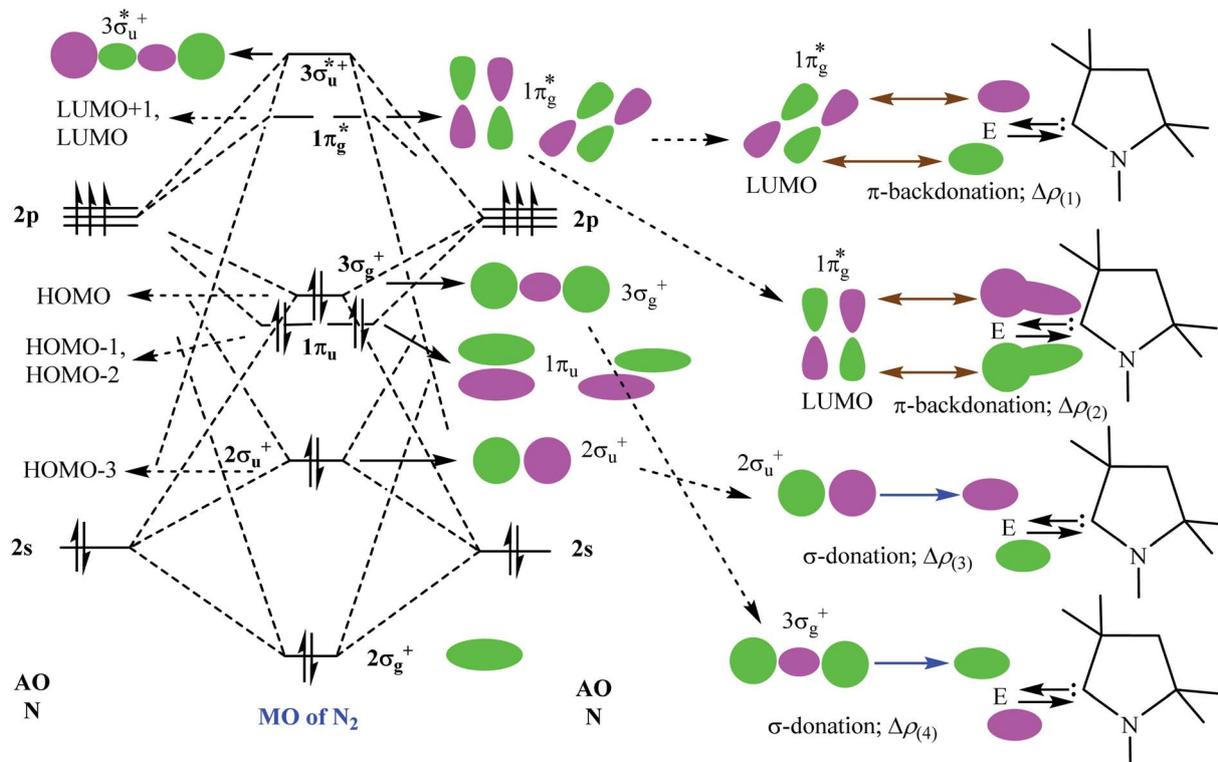
Fig. 9 Bonding and anti-bonding molecular orbitals of free N_2 molecule (left). The pairwise orbital interactions between few bonding and anti-bonding molecular orbitals of N_2 fragment with one of the cAAC^{Me}–Ge fragments (right; for simplification one is shown).

and S3† to illustrate the changes in the geometries at the key steps (higher energy local minima) until the final global minima (optimized geometry). The energies of the geometries at key steps (Fig. S2 and S3†) were calculated relative to the energy of the optimized geometry. The central Si=Si unit[38,39a,57] of the reported cAAC^{Dip}–Si=Si–cAAC^{Dip} showed the presence of different conformers in the solid state while in solution it maintains an average equilibrium geometry which has been studied by solid state/solution ^{29}Si NMR and temperature dependent X-ray structure determination.[57] At 23 K the cyclohexyl functionalized cAAC^{Dip} analogue Cy–cAAC^{Dip}–Si=Si–Cy–

cAAC^{Dip} possesses a centre of inversion between two Si-atoms while the molecule is non centero-symmetric at 100 K.[38] Thus, the central E–N–N–E unit of 1^{Dip}–2^{Dip} [(cAAC^{Dip}–Si)$_2$(N$_2$) (1^{Dip}), (cAAC^{Dip}–Si)$_2$(N$_2$) (2^{Dip})] may also possess some thermal movement around its equilibrium position in between two cAAC ligands. The void space around E–N–N–E unit may allow it to have some thermal movement.

The cAAC ligands with a Dip-group on the N-atom (Dip = 2,4-isopropylphenyl; cAAC^{Dip}) are regularly employed as an efficient coordinating/anchoring ligand.[36–39] The bonding and stability remain almost unaltered if the geometries of the species with
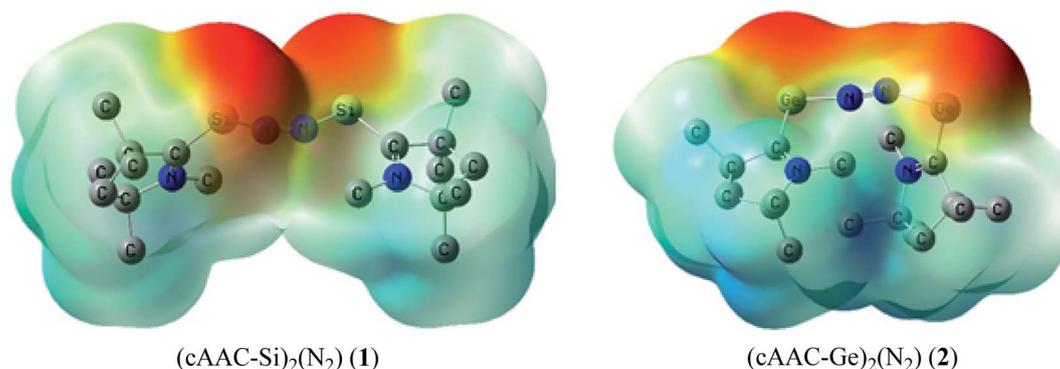

Fig. 10 Calculated MESP maps for the complexes (**1–2**) on optimized coordinates at DFT level using BP86-D3(BJ)/TZ2P method. Different colours show different electronegative regions; red is the most nucleophilic while dark blue is the most electrophilic region and yellow, green and light blue are in between.
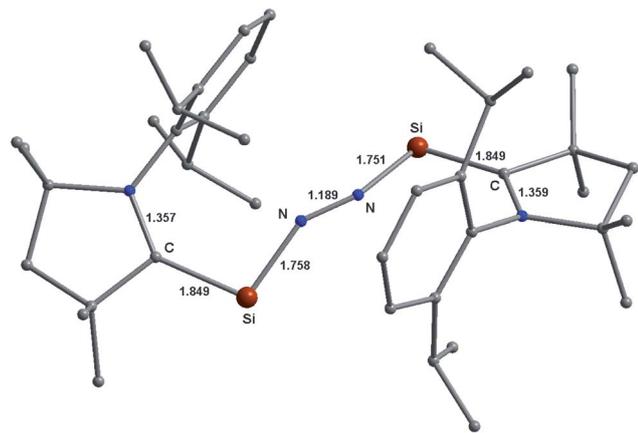
Fig. 11 Optimized equilibrium geometries of $(cAAC^{Dip}-Si)_2(N_2)$ ($\mathbf{1^{Dip}}$) in the singlet state at the BP86-D3(BJ)/TZ2P level of theory.

smaller substituents on the cAAC ligand do not change significantly on choosing smaller substituents on cAAC part for simplification. The Si-analogue of **1** (cAAC = cAAC^{Me}) having a Dip-group (cAAC = cAAC^{Dip}) on cAAC has been optimized in the same level of theory $[(cAAC^{Dip}-Si)_2(N_2)$ ($\mathbf{1^{Dip}}$)]. The central Si–N–N–Si non-linear chain of $\mathbf{1^{Dip}}$ has been shielded by two cAAC^{Dip} ligands (see space filling model in Fig. 11 and S4†). The cAAC^{Dip} ligands are oriented nearly *trans* (C_{cAAC}–Si–Si–C_{cAAC} torsion of 152.67° in $\mathbf{1^{Dip}}$ *vs.* 107.81° in **1**) to each other with respect to the central Si–N–N–Si chain. The C_{cAAC}–Si–N angle widens by 3° (100.89° in $\mathbf{1^{Dip}}$ *vs.* 97.4/97.6° in **1**). The bond length slightly changes at third decimal suggesting that the Si–N$_2$ interaction energies (ΔE_{int}) of $\mathbf{1^{Dip}}$ is expected to be very close to that of **1**. C–H$_{iPr}$···N weak interactions are observed (2.479/ 2.543 Å; see Fig. 11) in $\mathbf{1^{Dip}}$. Further calculations indicate that the cAAC^{Dip} ligands of $\mathbf{2^{Dip}}$ $[(cAAC^{Dip}-Si)_2(N_2)$ ($\mathbf{2^{Dip}}$)] also arrange themselves *trans* to each other with respect to the central Ge–N–N–Ge unit like Si-compound.

The precursor $(Me/Cy-cAAC^{Dip})SiCl_4$ has been reduced with KC$_8$ in different molar ratios to produce $(Me/Cy-cAAC^{Dip})SiCl_3$ radical, $(Me/Cy-cAAC^{Dip})_2Si_2Cl_4$, $(Me/Cy-cAAC^{Dip})_2Si_2Cl_2$, (Me/Cy-cAAC$^{Dip})_2Si_2$ in THF controlling the initiation temperatures of the reactions.[38] The $(Me/Cy-cAAC^{Dip})GeCl_2$ is isolated in small quantity by directly reacting GeCl$_2$(dioxane) adduct with cAAC ligand in the presence of an anionic compound to avoid the formation of cAACH$^+$ GeCl$_3^-$.[58] The adduct (bulky group-cAAC$^{bulky\ group})SiCl_4$ can be utilized as a precursor under reduced (KC$_8$) condition to prevent the dimerization of (bulky group-cAAC$^{bulky\ group})Si$ unit under dinitrogen atmosphere. In recent time, several bulky cAAC ligands[59,60] have been synthesized, isolated and utilized for catalytic organic transformation.[60] The bulky substituents around C_{cAAC}-atom is suggested here to prevent the dimerization of 2cAAC–E to (cAAC–E)$_2$ creating the possibility of N$_2$ binding by two cAAC–E fragments under suitable reaction condition *via* the prevention of self dimerization of 2 cAAC–E units. The later process is thermodynamically more favourable over binding of N$_2$ by 2 cAAC–E units.

Conclusion

The stability and bonding of N$_2$-bonded species (cAAC–E)$_2$(N$_2$) (**1–2**; Si, Ge) have been studied by DFT calculations [NBO, QTAIM and EDA-NOCV analyses]. The cAAC bonded E(0) [cAAC–E; E = Si, Ge] can act as a very good π-donor ligand. The major stability of E–N$_2$–E bonds in **1–2** arise from stronger π-back-donations (E → N$_2$; cAAC–E → N$_2$ ← E–cAAC) which are nearly 1.5 (Si) and 3 (Ge) times higher than σ-donations (E ← N$_2$; cAAC–E ← N$_2$ → E–cAAC) in **1** and **2**, respectively. The bonding interactions have been clearly shown in Fig. 8 and 9. The σ-charge polarization from E to N$_2$ is not negligible. The London dispersion force is only 1–2% of the total stabilization energy. Significant intrinsic interaction energies (~68–70 kcal mol^{-1}) of E–N E–N$_2$–E bonds in **1–2** suggest that species **1–2** may be synthesized and isolated in the laboratory.

Conflicts of interest

Authors do not have any conflict of interest.

Acknowledgements

References

1 C. Shan, S. Yao and M. Driess, *Chem. Soc. Rev.*, 2020, **49**, 6733.

2 (*a*) J. Cribb, *Surviving the 21st Century, Humanity's Ten Great Challenges and How We Can Overcome Them*, Springer International Publishing, 2017, eBook ISBN 978-3-319-41270-2; (*b*) R. Walsh, *Staying Alive: The Psychology of Human Survival*, 1984, New Science Library, USA, Boston, Massachusetts, U.S.A, 1984-09 ISBN 13: 9780394726908.

3 (*a*) A. Marshall, Development and Imperialism in Space, *Space Policy*, 1995, 11, pp. 41–52; (*b*) D. Deudney, *Dark Skies: Space Expansionism, Planetary Geopolitics, and the Ends of Humanity*, Oxford University Press, 2020, ISBN 978-0-19-009024-1. OCLC 1145940182.

4 J. A. Kent. *Riegel's Handbook of Industrial Chemistry*, CBS Publishers & Distributors, January 1, 1997, ISBN-13: 978-8123905440.

5 (*a*) A. W. Pierpont and T. R. Cundari, *J. Coord. Chem.*, 2011, **64**, 3123; (*b*) A. Nandy and H. J. Kulik, *ACS Catal.*, 2020, **10**, 15033; (*c*) Y. Nishibayashi, *Transition Metal-Dinitrogen Complexes: Preparation and Reactivity*, John Wiley & Sons, ISBN: 978-3-527-34425-3, 2019, 352734425X, 9783527344253.

6 (*a*) B. K. Burgess and D. J. Lowe, *Chem. Rev.*, 1996, **96**, 2983; (*b*) V. Smil, *Enriching the Earth: Fritz Haber, Carl Bosch and the Transformation of World Food Production*, MIT Press, Cambridge, 2001.

7 B. M. Hoffman, D. R. Dean and L. C. Seefeldt, *Acc. Chem. Res.*, 2009, **42**, 609.

8 J. L. Crossland and D. R. Tyler, *Coord. Chem. Rev.*, 2010, **254**, 1883.

9 (a) M. Appl, *The Haber–Bosch Process and the Development of Chemical Engineering. A Century of Chemical Engineering*, Plenum Press, New York, 1982, pp. 29–54, ISBN 978-0-306-40895-3; (b) P. H. Pfromm, *J. Renewable Sustainable Energy*, 2017, **9**, 034702.

10 (a) C.-H. Wang, Z.-B. Yin, J. Wei, W. X. Zhang and Z. Xi, *Tetrahedron*, 2020, **76**, 131703; (b) H. Song and E. Lee, *Chem.–Asian J.*, 2021, **16**, 2421–2425; (c) Q. Zhu, R. Qiu, S. Dong, G. Zeng and J. Zhu, *Chem.–Asian J.*, 2021, **16**, 2063–2067; (d) X. Yu, P. Han, Z. Wei, L. Huang, Z. Gu, S. Peng, J. Ma and G. Zheng, *Joule*, 2018, **2**, 1610–1622; (e) A. M. Rouf, C. Dai, S. Dong and J. Zhu, *Inorg. Chem.*, 2020, **59**, 11770–11781; (f) A. M. Rouf, Y. Huang, S. Dong and J. Zhu, *Inorg. Chem.*, 2021, **60**, 5598–5606.

11 (a) Z.-J. Lv, J. Wei, W.-X. Zhang, P. Chen, D. Deng, Z.-J. Shi and Z. Xi, *Natl. Sci. Rev.*, 2020, **7**, 1564; (b) S. Kin, F. Loose and P. J. Chirik, *Chem. Rev.*, 2020, **120**, 5637–5681; (c) R. J. Burford, A. Yaeo and M. D. Fryzuk, *Coord. Chem. Rev.*, 2017, **334**, 84–99; (d) R. J. Burford and M. D. Fryzuk, *Nat. Rev. Chem.*, 2017, **1**, 26; (e) H.-P. Jia and E. A. Quadrelli, *Chem. Soc. Rev.*, 2014, **43**, 547–564.

12 (a) T. Yamabe, K. Hori, T. Minato and K. Fukui, *Inorg. Chem.*, 1980, **19**, 2154–2159; (b) D. L. M. Suess, C. Tsay and J. C. Peters, *J. Am. Chem. Soc.*, 2012, **134**, 14158–14164; (c) M. T. Whited, N. P. Mankad, Y. Lee, P. E. Oblad and J. C. Peters, *Inorg. Chem.*, 2009, **48**, 2507.

13 B. D. Matson and J. C. Peters, *ACS Catal.*, 2018, **8**, 1448.

14 J. Fajardo, Jr and J. C. Peters, *J. Am. Chem. Soc.*, 2017, **139**, 16105.

15 J. Rittle and J. C. Peters, *Proc. Natl. Acad. Sci. U. S. A.*, 2013, **110**, 15898.

16 N. P. Mankad, M. T. Whited and J. C. Peters, *Angew. Chem., Int. Ed.*, 2007, **46**, 5768.

17 Y. Lee, N. P. Mankad and J. C. Peters, *Nat. Chem.*, 2010, **2**, 558.

18 S. E. Creutz and J. C. Peters, *J. Am. Chem. Soc.*, 2014, **136**, 1105.

19 M. D. Zott and J. C. Peters, *J. Am. Chem. Soc.*, 2021, **143**, 7612–7616.

20 N. B. Thompson, M. T. Green and J. C. Peters, *J. Am. Chem. Soc.*, 2017, **139**, 15312.

21 Q. J. Bruch, G. P. Connor, N. D. McMillion, A. S. Goldman, F. Hasanayn, P. J. Holland and A. J. M. Miller, *ACS Catal.*, 2020, **10**, 10826.

22 G. Ung and J. C. Peters, *Angew. Chem., Int. Ed.*, 2015, **54**, 532.

23 P. J. Hill, L. R. Doyle, A. D. Crawford and W. K. Myers, *J. Am. Chem. Soc.*, 2016, **138**, 13521.

24 T. A. Bazhenova and A. E. Shilov, *Coord. Chem. Rev.*, 1995, **144**, 69.

25 S. Kuriyama, K. Arashiba, K. Nakajima, Y. Matsuo, H. Tanaka, K. Ishii, K. Yoshizawa and Y. Nishibayashi, *Nat. Commun.*, 2016, **7**, 12181.

26 S. F. McWilliams, D. L. J. Broere, C. J. V. Halliday, S. M. Bhutto, B. Q. Mercado and P. L. Holland, *Nature*, 2020, **584**, 221.

27 Y. Lee, F. T. Sloane, G. Blondin, K. A. Abboud, R. García-Serres and L. J. Murray, *Angew. Chem., Int. Ed.*, 2015, **54**, 1499.

28 I. Čorić and P. L. Holland, *J. Am. Chem. Soc.*, 2016, **138**, 7200.

29 L. A. Wickramasinghe, T. Ogawa, R. R. Schrock and P. Müller, *J. Am. Chem. Soc.*, 2017, **139**, 9132.

30 B. M. Lindley, R. S. van Alten, M. Finger, F. Schendzielorz, C. Würtele, A. J. M. Miller, I. Siewert and S. Schneider, *J. Am. Chem. Soc.*, 2018, **140**, 7922.

31 Y. Sekiguchi, K. Arashiba, H. Tanaka, A. Eizawa, K. Nakajima, K. Yoshizawa and Y. Nishibayashi, *Angew. Chem., Int. Ed.*, 2018, **57**, 9064.

32 Y. Yao, S. Zhu, H. Wang, H. Li and M. Shao, *J. Am. Chem. Soc.*, 2018, **140**, 1496.

33 S. Ye, E. Bill and F. Neese, *Inorg. Chem.*, 2016, **55**, 3468.

34 R. Bjornsson, F. Neese and S. DeBeer, *Inorg. Chem.*, 2017, **56**, 1470.

35 I. Čorić, B. Q. Mercado, E. Bill, D. J. Vinyard and P. L. Holland, *Nature*, 2015, **526**, 96.

36 (a) E. Welz, I. Krummenacher, B. Engels and H. Braunschweig, *Science*, 2018, **359**, 896; (b) M. A. Légaré, M. Rang, G. Bélanger-Chabot, J. I. Schweizer, I. Krummenacher, R. Bertermann, M. Arrowsmith, M. C. Holthausen and H. Braunschweig, *Science*, 2019, **363**, 1329; (c) M. A. Legare, G. Belanger-Chabot, M. Rang, R. D. Dewhurst, I. Krummenacher, R. Bertermann and H. Braunschweig, *Nat. Chem.*, 2020, **12**, 1076; (d) H. Braunschweig, I. Krummenacher, M. A. Legare, A. Matler, K. Radacki and Q. Ye, *J. Am. Chem. Soc.*, 2017, **139**, 1802.

37 V. Lavallo, Y. Canac, C. Präsang, B. Donnadieu and G. Bertrand, *Angew. Chem., Int. Ed.*, 2005, **44**, 5705.

38 K. C. Mondal, S. Roy and H. W. Roesky, *Chem. Soc. Rev.*, 2016, **45**, 1080.

39 (a) K. C. Mondal, P. P. Samuel, H. W. Roesky, R. R. Aysin, L. A. Leites, S. Neudeck, J. Lübben, B. Dittrich, M. Hermann and G. Frenking, *J. Am. Chem. Soc.*, 2014, **136**, 8919; (b) K. C. Mondal, S. Roy, B. Dittrich, D. M. Andrada, G. Frenking and H. W. Roesky, *Angew. Chem., Int. Ed.*, 2016, **55**, 3158.

40 L. Zhao, S. Pan, N. Holzmann, P. Schwerdtfeger and G. Frenking, *Chem. Rev.*, 2019, **119**, 8781.

41 (a) G. Frenking and F. M. Bickelhaupt, *The Chemical Bond 1. Fundamental Aspects of Chemical Bonding*, chap. The EDA Perspective of Chemical Bonding, Wiley-VCH, Weinheim, 2014, vol 121; (b) L. M. Zhao, M. von Hopffgarten, D. M. Andrada and G. Frenking, *Wiley Interdiscip. Rev.: Comput. Mol. Sci.*, 2018, **8**, 1345; (c) L. Zhao, M. Hermann, W. H. E. Schwarz and G. Frenking, *Nat. Rev. Chem.*, 2019, **3**, 48; (d) S. Pan and G. Frenking, *Angew. Chem., Int. Ed.*, 2020, **59**, 8756; (e) J. Andrés, P. W. Ayers, R. A. Boto, R. Carbó-Dorca, H. Chermette, J. Cioslowski, J. Contreras-García, D. L. Cooper, G. Frenking, C. Gatti, F. Heidar-Zadeh, L. Joubert, Á. M. Pendás, E. Matito, I. Mayer, A. J. Misquitta, Y. Mo, J. Pilmé, P. L. A. Popelier, M. Rahm, E. Ramos-Cordoba, P. Salvador, W. H. E. Schwarz, S. Shahbazian, B. Silvi, M. Solà, K. Szalewicz, V. Tognetti, F. Weinhold and É. L. Zins, *J. Comput. Chem.*, 2019, **40**, 2248; (f) W. Yang, K. E. Krantz, L. A. Freeman, D. Dickie, A. Molino, G. Frenking, S. Pan, D. J. D. Wilson and

R. J. Gilliard, Jr, *Angew. Chem., Int. Ed.*, 2020, **59**, 3850; (*g*) S. M. N. V. T. Gorantla, P. Parameswaran and K. C. Mondal, *J. Comput. Chem.*, 2021, **42**, 1159; (*h*) S. M. N. V. T. Gorantla, S. Pan, K. C. Mondal and G. Frenking, *Chem.–Eur. J.*, 2020, **26**, 14211; (*i*) L. Zhao, S. Pan, M. Zhou and G. Frenking, *Science*, 2019, **365**, eaay5021; (*j*) R. Saha, S. Pan, P. K. Chattaraj and G. Merino, *Dalton Trans.*, 2020, **49**, 1056.

42 R. Tonner and G. Frenking, *Angew. Chem., Int. Ed.*, 2007, **46**, 8695.

43 (*a*) C. A. Dyker, V. Lavallo, B. Donnadieu and G. Bertrand, *Angew. Chem. Int. Ed.*, 2008, **47**, 3206; (*b*) A. Fürstner, M. Alcarazo, R. Goddard and C. W. Lehmann, *Angew. Chem., Int. Ed.*, 2008, **47**, 3210.

44 (*a*) M. A. Celik, R. Sure, S. Klein, R. Kinjo, G. Bertrand and G. Frenking, *Chem.–Eur. J.*, 2012, **18**, 5676; (*b*) H. Braunschweig, R. D. Dewhurst, F. Hupp, M. Nutz, K. Radacki, C. W. Tate, A. Vargas and Q. Ye, *Nature*, 2015, **522**, 327.

45 (*a*) A. D. Becke, *Phys. Rev. A*, 1988, **38**, 3098–3099; (*b*) J. P. Perdew, *Phys. Rev. B: Solid State*, 1986, **33**, 8822–8823; (*c*) S. Grimme, S. Ehrlich and L. Goerigk, *J. Comput. Chem.*, 2011, **32**, 1456–1465; (*d*) S. Grimme, J. Antony, S. Ehrlich and H. A. Krieg, *J. Chem. Phys.*, 2010, **132**, 154104; (*e*) F. Weigend and R. Ahlrichs, *Phys. Chem. Chem. Phys.*, 2005, **7**, 3297; (*f*) F. Weigend, *Phys. Chem. Chem. Phys.*, 2006, **8**, 1057.

46 M. J. Frisch, *et al.*, *Gaussian 16, Revision A.03*, Gaussian, Inc., Wallingford CT, 2016.

47 (*a*) F. Weinhold and C. Landis, *Valency and Bonding, A Natural Bond Orbital Donor – Acceptor Perspective*, Cambridge University Press, Cambridge, 2005; (*b*) C. R. Landis and F. Weinhold, *The NBO View of Chemical Bonding. The Chemical Bond: Fundamental Aspects of Chemical Bonding*, ed. G. Frenking and S. Shaik, Wiley-VCH, Weinheim, 2014, pp. 91–120; (*c*) F. M. Bickelhaupt and E. J. Baerends, Kohn-Sham Density Functional Theory: Predicting and Understanding Chemistry, in *Rev. Comput. Chem.*, ed. K. B. Lipkowitz and B. D. Boyd, Wiley-VCH, New York, 2000, vol. 15, pp. 1–86.

48 K. B. Wiberg, *Tetrahedron*, 1968, **24**, 1083–1096.

49 T. Ziegler and A. Rauk, *Theor. Chim. Acta*, 1977, **46**, 1–10.

50 (*a*) M. Mitoraj and A. Michalak, *Organometallics*, 2007, **26**, 6576–6580; (*b*) M. Mitoraj and A. Michalak, *J. Mol. Model.*, 2008, **14**, 681–687.

51 (*a*) ADF2017, SCM, *Theoretical Chemistry*, Vrije Universiteit, Amsterdam, The Netherlands, http://www.scm.com; (*b*) G. te Velde, F. M. Bickelhaupt, E. J. Baerends, C. F. Guerra, S. J. A. van Gisbergen, J. G. Snijders and T. Ziegler, *J. Comput. Chem.*, 2001, **22**, 931.

52 (*a*) E. van Lenthe and E. J. Baerends, *J. Comput. Chem.*, 2003, **24**, 1142; (*b*) E. van Lenthe, E. J. Baerends and J. G. Snijders, *J. Chem. Phys.*, 1993, **99**, 4597; (*c*) E. van Lenthe, E. J. Baerends and J. G. Snijders, *J. Chem. Phys.*, 1994, **101**, 9783.

53 P. S. V. Kumar, V. Raghavendra and V. Subramanian, *J. Chem. Sci.*, 2016, **128**, 1527.

54 S. Jenkins, L. Blancafort, S. R. Kirk and M. J. Bearpark, *Phys. Chem. Chem. Phys.*, 2014, **16**, 7115.

55 N. Holzmann, D. M. Andrada and G. Frenking, *J. Orgmet. Chem.*, 2015, **792**, 139.

56 A. Sidiropoulos, C. Jones, A. Stasch, S. Klein and G. Frenking, *Angew. Chem., Int. Ed.*, 2009, **48**, 9701.

57 K. C. Mondal, S. Roy, B. Dittrich, B. Maity, S. Dutta, D. Koley, S. K. Vasa, R. Linser, S. Decherta and H. W. Roesky, *Chem. Sci.*, 2015, **6**, 5230.

58 Y. Li, K. C. Mondal, H. W. Roesky, H. Zhu, P. Stollberg, R. Herbst-Irmer, D. Stalke and D. M. Andrada, *J. Am. Chem. Soc.*, 2013, **135**, 12422.

59 D. Pichon, M. Soleilhavoup, J. Morvan, G. P. Junor, T. Vives, C. Crévisy, V. Lavallo, J.-M. Campagne, M. Mauduit, R. Jazzar and G. Bertrand, *Chem. Sci.*, 2019, **10**, 7807.

60 J. Morvan, M. Mauduit, G. Bertrand and R. Jazzar, *ACS Catal.*, 2021, **11**, 1714.